IEEE Access
Multidisciplinary | Rapid Review | Open Access Journal

Received April 13, 2021, accepted April 20, 2021, date of publication April 23, 2021, date of current version May 3, 2021.

Digital Object Identifier 10.1109/ACCESS.2021.3075206

In-Plane Nonlinear Vibration of Overhead Power Transmission Conductors With Coupling Effects of Wind and Rain

CHAO ZHOU
School of Energy, Power and Mechanical Engineering, North China Electric Power University, Beijing 102206, China
e-mail: zhouchao@ncepu.edu.cn

This work was supported in part by the National Key Research and Development Program of China under Grant 2018YFC0809400, in part by the National Natural Science Foundation of China under Grant 52075169, and in part by the Beijing Natural Science Foundation under Grant 8202043.

ABSTRACT In this paper a small sag-to-span ratio conductor, belonging to overhead power transmission conductors, is studied. The single conductor is assumed to withstand a prescribed motion at a single conductor ends caused by suspended insulator swing and placed in the simultaneous wind and rain condition. It is modeled as a planar, nonlinear, one-dimensional continuum, and its ends are assumed to undergo the suspended insulator swing of given amplitude and frequency. Raindrops are blowing by uniformed wind flow, hitting the single conductor and may form rivulets on its surface. Besides rain-wind flow induces aerodynamic instability, the motions of the suspended insulator swing contribute to external and parametric excitation. Vertical motion equation of the single conductor is discretized with Galerkin method of which first order in-plane symmetric mode is took as trial function. Multiple-scale perturbation technique and computation methods are introduced to study nonlinear dynamic responses of the single conductor under parametric excitation or force excitation, or both excitations. Effects of key parameters, such as total damping ratio, upper rivulet angle, suspended insulator swing amplitude and frequency on dynamic characteristics of the single conductor are discussed. The results indicated that those key-parameters have obviously affected the dynamic characteristics of high-voltage conductor.

INDEX TERMS Overhead power transmission conductor, sub-harmonic resonance, upper rivulet, rain-wind flow.

I. INTRODUCTION

Overhead power transmission conductors are prone to vibrate due to their structural flexible and sensitive to external loads or tip motion. There are a few of research about this type of unanticipated nonlinear vibrations for the conductors under coupling action of wind and rain [1]–[3]. Such large amplitude vibrations make the conductors stress undue, and produce metal fatigue, especially on conductor supports or clamps, in surprisingly short periods. Therefore, it is urgently needing an in-depth investigation to reveal mechanism behind such a vibration.

The dynamic behaviors of the overhead power transmission conductors under rain-wind condition are very complicated and have attracted increasing amount of attention from electrical, mechanics and mechanical engineering.

The associate editor coordinating the review of this manuscript and approving it for publication was Hassen Ouakad.

Wang and Tang [4] proposed a partial differential equation of nonlinear vibration of suspended power line in consideration of initial relaxation degree and obtained the nonlinear vibration response under harmonic forces and pulse excitation. Rienstra [5] studied nonlinear free vibration of coupled spans of suspended overhead transmission lines. It is shown that the natural vibration is the gravity model, of which the tension component vanishes in the first harmonic. Barbieri *et al.* [6] analyzed nonlinear characteristics of the large amplitude free vibrations of non-inclined and inclined sagged elastic transmission lines with finite element method and validated the nonlinear models with experimental data. Xia *et al.* [7] established a finite element model of a domestic 500kV high-voltage tower-line system to study the nonlinear dynamic response under mechanical failure. Wu [8] studied a class of nonlinear vibration model of a transmission line and obtained an approximate solution with an arbitrary degree of accuracy. Yan *et al.* [9] modeled the galloping of iced transmission

line considering eccentricity and analyzed the bifurcation and stability of 1:1 and 2:1 resonance. Liu and Huo [10] developed a model of iced transmission line with thin ice accretions to describe the nonlinear interactions between the in-plane, out-of-plane and torsional vibration, and observed Hopf bifurcation, mono-modal, bi-modal and multi-modal galloping. Wang *et al.* [11] estimated the buffeting response of overhead conductor based on random vibration theory with closed form formulations and placed special attention on the influenced of geometric non-linearity. Zhang *et al.* [12] established a 3-DOF model of transmission line with initial deflection and studied the nonlinear-coupled in-plane and out-of-plane internal resonance. Alminhana *et al.* [13] developed a special-purpose nonlinear dynamic analysis technique for the modeling of multi-span line sections under progressive failure scenarios. Burgh and Harton [14], Burgh *et al.* [15] presented a model equation for the study of rain-wind induced vibrations of a simple oscillator and found that variations of the detuning parameter will lead to saddle-node and Hopf bifurcations. Fu and Li [16], [17] established the calculating method of wind and rain loads for transmission conductor and discussed the effects of wind and rain excitation, and the results indicated that the rain loads relative to the wind loads could reach to 22%. Zhou *et al.* [18], [19] developed a two-dimensional model of rain-wind induced vibration of transmission line and discussed aerodynamic instability zone with Lyapunov stability criterion.

Compared with the dynamics of the overhead power transmission conductors subjected to parametric excitation or force excitation, or both excitation, nonlinear investigation towards the mechanism of rain-wind induced conductor vibration are still insufficient. Though nonlinear dynamics of suspended horizontal and inclined cables subjected to wind and rain loads are studied [20]–[23], the structural characteristics, cross-sectional dimension between the stayed cables and the conductors are clearly different. Thus, there is an urgent need to reveal the in-plane nonlinear characteristics of the conductors, especially first- order symmetric in-plane mode under parametric and aerodynamic excitation. The paper is organized as follows: in section 2, equations of the single conductor motion are presented and discretized. In section 3, the perturbation analysis is carried out and the amplitude modulation equation is derived. In section 4, these latter are numerical computed for a sample example. Finally, the paper ends with some conclusions.

II. GOVERNING EQUATIONS

A. BASIC CONFIGURATIONS

The overhead power transmission conductors made of a sequence of several spans, and each span ends hinge-supported with anchoring or suspension insulator. The overhead transmission line is model as a single conductor with sag-to-span ratio about 1:8 or less, having its weight expressed by mass per unit of length, m, subject to tension H. A Cartesian coordinate system Oxy is used here to identify

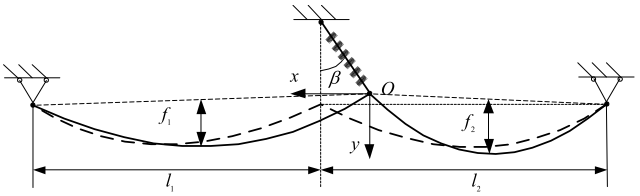

FIGURE 1. Configuration of conductor-insulator structure with two-span.

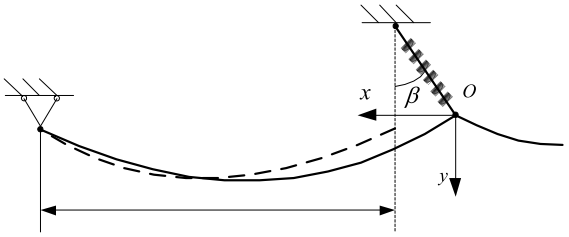

FIGURE 2. Substructure of conductor-insulator.

motions of the single conductor, with original point O located at the end of the middle suspension insulator. The geometrical configuration of a conductor-insulator structure with two-span (see Fig. 1), and the static profile be defined by a parabolic function as

$$y = 4f_i(x/l_i - x^2/l_i^2) \quad i = 1, 2 \tag{1}$$

where l_1, l_2 are the span of first-span conductor and second-span conductor, respectively. f_1, f_2 are the sage of first-span conductor and second-span conductor.

The flexural, torsional, and shear stiffness of the single conductor is negligible, for brevity, will be neglected in the following studies. Moreover, the motion of the suspended insulator swing be simplified defined as a harmonic excitation acts on the end of single conductor. Therefore, in-plane motion equations of the single conductor based on Hamilton's theory, are derived as

$$\frac{\partial}{\partial x}\left(EA\left[\frac{\partial u}{\partial x} + \frac{\partial v}{\partial x}\frac{dy}{dx} + \frac{1}{2}\left(\frac{\partial v}{\partial x}\right)^2\right]\right) - m\ddot{u} + F_x = 0 \tag{2}$$

$$\frac{\partial}{\partial x}\left(H\frac{\partial v}{\partial x} + EA\left(\frac{\partial v}{\partial x} + \frac{dy}{dx}\right)\left[\frac{\partial u}{\partial x} + \frac{\partial v}{\partial x}\frac{dy}{dx} + \frac{1}{2}\left(\frac{\partial v}{\partial x}\right)^2\right]\right) - m\ddot{v} + F_y = 0 \tag{3}$$

where F_x and F_y are the external forces. A is cross sectional area of the single conductor, and E is Young's modulus. u and v are axial and vertical motion at point x and time t from the static equilibrium, respectively. The dot is the derivative with respect to time t.

In order to reveal the interaction between each span of the single conductor vibration, we select the first-span conductor and the suspended insulator as substructure. The effect of the second-span conductor movement to the substructure is equivalent to the motion of the suspended insulator (see Fig. 2).

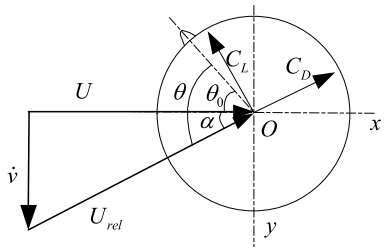

FIGURE 3. Aerodynamic force exerted on the surface of the single conductor.

Assumed that the tangential excitation is acted to the first-span conductor, caused by swing of the suspended insulator as

$$s(t) = Bcos\omega_b t \tag{4}$$

where $B = b\sqrt{2(1-cos\beta)}$ is the tangential amplitude, b is length of the insulator, and β is yaw angle.

Thus, the connection conditions between the first-span conductor and the tangential excitation can be expressed as:

$$u(0,t) - s(t)\cos\beta = 0, \quad v(0,t) - s(t)\sin\beta = 0 \tag{5}$$

From the Fig. 2, it can be seen that the boundary conditions on the left side of the first-span conductor, axial motion u and vertical motion v can be given by

$$u(l_1,t) = 0, \quad v(l_1,t) = 0 \tag{6}$$

Given that ratio of transverse-to-longitudinal squared frequency get a small value and the interaction between axial displacement and vertical displacement is negligible, the inertial and damping terms are neglected in Eq. (2). Thus, the axial displacement is statically condensed as

$$\frac{\partial u}{\partial x} + \frac{\partial v}{\partial x}\frac{dy}{dx} + \frac{1}{2}\left(\frac{\partial v}{\partial x}\right)^2 = -\frac{u(0,t)}{l_1} + \frac{1}{l_1}\int_0^{l_1}\left(\frac{\partial v}{\partial x}\frac{dy}{dx} + \frac{1}{2}\left(\frac{\partial v}{\partial x}\right)^2\right)dx \tag{7}$$

Substitute Eq. (7) into Eq. (3), one can obtain

$$EA\frac{\partial}{\partial x}\left(\frac{\partial v}{\partial x} + \frac{dy}{dx}\right)\left(-\frac{u(0,t)}{l_1} + \frac{1}{l_1}\int_0^{l_1}\left(\frac{\partial v}{\partial x}\frac{dy}{dx} + \frac{1}{2}\left(\frac{\partial v}{\partial x}\right)^2\right)dx\right) + H\frac{\partial^2 v}{\partial x^2} - m\ddot{v} + F_y = 0 \tag{8}$$

B. RAIN-WIND MODEL OF THE SINGLE CONDUCTOR

An available rain-wind model of the single conductor, allowing one to obtain the expression for the aerodynamic force F_y in Eq. (3), is introduced as the one presented in [24]. It describes the aerodynamic force F_y exerted on the surface of the single conductor with upper rivulet (radius ratio $r/R = 0.1$). The single conductor is capable of in-plane motion and withstand to an horizontal uniform wind of velocity U, as shown in Fig. 3.

Based on some appropriate assumptions, quasi-steady theory is adopted, the axial flow and axial vortexes along the single conductor be neglected, whereas an upper rivulet is presented on the surface of the single conductor. When the single conductor moves in the positive y with velocity $\dot{v}$, the relative wind velocity U_{rel} can be obtained with angle of attack α. The upper rivulet position θ on the surface of the single conductor is varies with time. From Fig. 3, it follows that

$$\begin{cases} sin\alpha = \dot{v}/U_{rel} \\ cos\alpha = U/U_{rel} \\ \theta = \theta_0 + arctan(\dot{v}/U) \end{cases} \tag{9}$$

On the basis of the quasi-steady theory, the aerodynamic force F_y exerts on the surface of the single conductor per unit length as:

$$F_y = -\rho R U^2\sqrt{1+(\dot{v}/U)^2}(C_D(\theta)\dot{v}/U + C_L(\theta)) \tag{10}$$

where ρ is the air density, and R is the radius of the single conductor. C_D, C_L are the drag and lift coefficients, respectively.

The aerodynamic coefficients C_D and C_L can be approximated by a constant and a cubic polynomial [25], respectively.

$$\begin{cases} C_D(\theta) = C_{D0} \\ C_L(\theta) = C_{L1}(\theta - \theta_0) + C_{L3}(\theta - \theta_0)^3 \end{cases} \tag{11}$$

where θ_0 is an angle in the domain of the θ, at which the slope curve of $C_L(\theta)$ is negative, that is, $C_L(\theta) < 0$.

By using Eq. (9) and Eq. (11) can be written as

$$\begin{cases} C_D(\theta) = C_{D0} \\ C_L(\theta) = C_{L1}(\theta + artan(\dot{v}/U)) \\ \qquad\qquad +C_{L3}(\theta + artan(\dot{v}/U))^3 \end{cases} \tag{12}$$

The motion of the upper rivulet, θ, can be assumed to be harmonic as the steady-state vibration is concerned by reference to the wind-rain tests [26]. Thus,

$$\theta = \bar{\theta} sin\omega_a t \tag{13}$$

where θ is the oscillation range of the upper rivulet. ω_a is the oscillation frequency of the upper rivulet, which is very close to that of the single conductor.

Substitute Eq. (12), (13) into Eq. (10), and expand the right-side with respect to $\dot{v}/U$ in the neighborhood of $\dot{v}/U \approx 0$ yields

$$F_y = -(f_0(\omega_a t) + f_1(\omega_a t)\dot{v} + f_2(\omega_a t)\dot{v}^2) + 0(\dot{v})^3 \tag{14}$$

where

$$\begin{cases} f_0(\omega_a t) = \rho R\bar{\theta} sin\omega_a t(C_{L1} + C_{L3}\bar{\theta}^2 sin^2\omega_a t) \\ f_1(\omega_a t) = \rho R U(C_{D0} + C_{L1} + 3C_{L3}\bar{\theta}^2 sin^2\omega_a t) \\ f_2(\omega_a t) = \rho R\bar{\theta} sin\omega_a t(C_{L1} + C_{L3}\bar{\theta} sin\omega_a t + 6C_{L3})/2 \end{cases}$$

C. QUASI-STATIC SOLUTION

Galerkin method is applied to solve Eq. (8), and the in-plane motion is expressed with a method of variables separable. Thus,

$$v(x,t) = s(t)\sin\beta(1 - x/l) + sin(\pi x/l)\phi(t) \tag{15}$$

where $\phi(t)$ time variation of $v(x,t)$, and l has been used to replace l_1 for brevity. It should be pointed out that first symmetric in-plane mode and the connection condition are taking into consideration.

Substitute Eq. (4), (12) and (14)into Eq. (8), and introducing viscous damping coefficients c. Correspondingly, a nonlinear ordinary differential equation is derived as:

$$\begin{aligned}
&\frac{1}{2}ml\ddot{\phi}(t) + \frac{1}{2}l(c + f_1(\omega_a t) + \frac{\omega_b Blsin\beta}{\pi}f_2(\omega_a t)sin\omega_b t)\dot{\phi}(t)\\
&+\frac{l^2}{4}f_2(\omega_a t)\dot{\phi}^2(t) + \left\{\frac{\pi^2 H}{2l} + \frac{\pi^2 B^2 EAsin^2\beta}{2l^3} + \frac{256f^2 EA}{\pi^2 l^3}\right.\\
&\left.+\frac{BEA\pi^2 cos\beta}{2l^2}cos\omega_b t + \frac{B^2 EA\pi^2 sin^2\beta}{2l^3}cos2\omega_b t\right\}\phi(t)\\
&+\frac{12f\pi EA}{l^3}\phi^2(t) + \frac{\pi^4 EA}{8l^3}\phi^3(t) + \frac{16B^2 fEAsin^2\beta}{\pi l^3}\\
&-\left\{\frac{mlB\omega_b^2}{\pi}sin\beta - \frac{16BfEA}{\pi l^2}cos\beta\right\}cos\omega_b t\\
&+\frac{16B^2 fEAsin^2\beta}{\pi l^3}cos2\omega_b t + \frac{2l}{\pi}f_0(\omega_a t)\\
&-\frac{\omega_b lBsin\beta}{\pi}f_1(\omega_a t)sin\omega_b t + \frac{2\omega_b^2 l^2 B^2 sin^2\beta}{\pi^2}f_2(\omega_a t)\\
&-\frac{\omega_b lBsin\beta}{\pi^2}f_2(\omega_a t)cos2\omega_b t = 0
\end{aligned} \tag{16}$$

The non-dimensional variables are defined as following:

$$\begin{cases}
\tau = \omega_0 t;\ \ q = \dfrac{\phi}{l};\ \ s = \dfrac{B}{l};\ \ k_a = \dfrac{\omega_a}{\omega_0};\ \ k_b = \dfrac{\omega_b}{\omega_0}\\
\omega_0 = \dfrac{\pi}{l}\sqrt{\dfrac{H}{m}};\ \ \xi_s = \dfrac{c}{2m\omega_0}\tilde{a}_1 = \dfrac{BEAcos\beta}{Hl};\\
\tilde{a}_2 = \dfrac{B^2 EAsin^2\beta}{4Hl^2};\ \ \omega_c = \sqrt{1 + \dfrac{B^2 EAsin^2\beta}{4Hl^2} + \dfrac{512f^2 EA}{Hl^2\pi^4}}\\
\tilde{a}_3 = \dfrac{24f\pi EA}{ml^4\omega_0^2};\ \ \tilde{a}_4 = \dfrac{\pi^4 EA}{4ml^4\omega_0^2};\ \ \tilde{a}_5 = \dfrac{32BfEA}{\pi ml^3\omega_0^2}cos\beta\\
-\dfrac{2B\omega_b^2}{\pi\omega_0^2}sin\beta\tilde{a}_6 = \tilde{a}_7 = \dfrac{8B^2 fEAsin^2\beta}{\pi ml^4\omega_0^2};\ \ \bar{a}_1' = \dfrac{1}{m\omega_0};\\
\bar{a}_2' = \dfrac{\omega_b Bsin\beta}{m\pi\omega_0};\ \bar{a}_3' = \dfrac{l}{2m}\ \bar{a}_4' = \dfrac{4}{m\pi\omega_0^2};\ \bar{a}_5' = \dfrac{2\omega_b Bsin\beta}{m\pi\omega_0^2};\\
\bar{a}_6' = \dfrac{4\omega_b^2 B^2 lsin^2\beta}{m\pi^2\omega_0^2};\ \ \bar{a}_7' = \dfrac{2\omega_b Bsin\beta}{m\pi^2\omega_0^2}
\end{cases} \tag{17}$$

Substituting them into Eq. (16) yields

$$\begin{aligned}
&\ddot{q} + \left\{2\xi_s + \bar{a}_1' f_1(k_a\tau) + \bar{a}_2' f_2(k_a\tau)sink_b\tau\right\}\dot{q} + \bar{a}_3' f_2(k_a\tau)\dot{q}^2\\
&+\left\{\omega_c^2 + \tilde{a}_1 cosk_b\tau + \tilde{a}_2 cos2k_b\tau\right\}q + \tilde{a}_3 q^2 + \tilde{a}_4 q^3\\
&+\tilde{a}_5 cosk_b\tau + (\tilde{a}_6 - \bar{a}_7' f_2(k_a\tau))cos2k_b\tau + \tilde{a}_7 + \bar{a}_4' f_0(k_a\tau)\\
&-\bar{a}_5' f_1(k_a\tau)sink_b\tau + \bar{a}_6' f_2(k_a\tau) = 0
\end{aligned} \tag{18}$$

where $\xi_a = \bar{a}_1' f_1(k_a\tau) + \bar{a}_2' f_2(k_a\tau)sink_b\tau$, ξ_a is aerodynamic damping ratio. $\xi = 2\xi_s + \bar{a}_1' f_1(k_a\tau) + \bar{a}_2' f_2(k_a\tau)sink_b\tau$, ξ is total damping ratio.

It can be found from Eq. (18) that self-, parametric and external excitation are noted, especially quadratic and cubic non-linearity occur else. The position of the upper rivulet θ relates to the aerodynamic lift and drag forces, which may cause a damping coupling and contributes to some nonlinear mechanical coefficients.

III. CASE STUDY PERTURBATION ANALYSIS WITH DYNAMICS OF SINGLE CONDUCTOR

Multiple-scale perturbation method is introduced here to study the dynamics of the single conductor. As quadratic and cubic terms appear in Eq. (18), three orders of perturbation equations are need. Let $T_i = \varepsilon^i\tau$, ε is a small factor. Apply the following scaling to Eq. (8),

$$\begin{aligned}
&\varepsilon^2\zeta = \xi_s, \varepsilon^2\bar{a}_1 = \bar{a}_1', \varepsilon^2\bar{a}_2 = \bar{a}_2', \bar{a}_3 = \bar{a}_3', \varepsilon^4\bar{a}_4 = \bar{a}_4',\\
&\varepsilon^5\bar{a}_5 = \bar{a}_5', \varepsilon^4\bar{a}_6 = \bar{a}_6', \varepsilon^2\bar{a}_7 = \bar{a}_7', \varepsilon^2 a_1 = \tilde{a}_1, \varepsilon^2 a_2 = \tilde{a}_2,\\
&a_3 = \tilde{a}_3, a_4 = \tilde{a}_4, \varepsilon^2 a_5 = \tilde{a}_5, \varepsilon^2 a_6 = \tilde{a}_6
\end{aligned}$$

It becomes of the following form

$$\begin{aligned}
&\ddot{q} + \varepsilon^2\left\{2\zeta + \bar{a}_1 f_1(k_a\tau) + \bar{a}_2 f_2(k_a\tau)sink_b\tau\right\}\dot{q} + \bar{a}_3 f_2(k_a\tau)\dot{q}^2\\
&+\left\{\omega_c^2 + \varepsilon^2 a_1 cosk_b\tau + \varepsilon^2 a_2 cos2k_b\tau\right\}q + a_3 q^2\\
&+a_4 q^3 + \varepsilon^2 a_5 cosk_b\tau + \varepsilon^2(a_6 - \bar{a}_7 f_2(k_a\tau))cos2k_b\tau\\
&+\varepsilon^4\bar{a}_4 f_0(k_a\tau) - \varepsilon^3\bar{a}_5 f_1(k_a\tau)sink_b\tau + \varepsilon^4\bar{a}_6 f_2(k_a\tau) = 0
\end{aligned} \tag{19}$$

Considering $T_i = \varepsilon^i\tau$, it has the differential operators

$$\begin{cases}
\dfrac{d}{d\tau} = D_0 + \varepsilon D_1 + \varepsilon^2 D_2 + \cdots\\
\dfrac{d^2}{d\tau^2} = D_0^2 + 2\varepsilon D_0 D_1 + \varepsilon^2(D_1^2 + 2D_0 D_2) + \cdots
\end{cases} \tag{20}$$

where $D_i = \partial/\partial T_i$.

Solutions of Eq. (19), can be expanded in the following form, in terms of a small positive parameter ε:

$$\begin{aligned}
q(T_0, T_2, \varepsilon) = \varepsilon q_0(T_0, T_2) + \varepsilon^2 q_1(T_0, T_2)\\
+\varepsilon^3 q_2(T_0, T_2) + \cdots
\end{aligned} \tag{21}$$

To define $\phi_j (j = 0, 1, 2)$, let the coefficients of ε, ε^2 and ε^3 be zero, and substitute Eq. (21) into Eq. (19). Thus,

Order ε

$$D_0^2 q_0 + \omega_c^2 q_0 = 0 \tag{22}$$

Order ε^2

$$\begin{aligned}
&D_0^2 q_1 + \omega_c^2 q_1 = -\bar{a}_3(D_0 q_0)^2 - a_3 q_0^2\\
&-(a_6 - \bar{a}_7 f_2(k_a T_0))cos(2k_b T_0) - a_5 cos(k_b T_0)
\end{aligned} \tag{23}$$

Order ε^3

$$\begin{aligned} &D_0^2 q_2 + \omega_c^2 q_2 \\ &= -2D_0 D_2 q_0 - a_1\phi_0 cos(k_b T_0) - 2a_3\phi_0\phi_1 \\ &\quad - [2\zeta + \bar{a}_1 f_1(k_a T_0) + \bar{a}_2 f_2(k_a T_0) sin(k_b T_0)] D_0 q_0 \\ &\quad - a_2\phi_0 cos(2k_b T_0) - a_4\phi_0^3 + \bar{a}_5 f_1(k_a T_0) sin(k_b T_0) \end{aligned} \quad (24)$$

First-order in-plane motion, derived by Eq. (22) as

$$q_0 = A(T_2) exp(i\omega_c T_0) + cc \quad (25)$$

where $exp(i\omega_c T_0) = e^{i\omega_c T_0}$, and cc is complex conjugate of other terms.

Substitute Eq. (25) into Eq. (23) gives

$$\begin{aligned} q_1 = &-\bar{a}_3 A^2 exp(2i\omega_c T_0)/3 + \bar{a}_3 A\bar{A} - 2a_3 A\bar{A}/\omega_c^2 \\ &+ a_3 A^2 exp(2i\omega_c T_0)/3\omega_c^2 + a_5\Gamma_1 exp(ik_b T_0)/2 \\ &+ (a_6 - \bar{a}_7 f_2(k_a T_0))\Gamma_2 exp(2ik_b T_0)/2 + cc \end{aligned} \quad (26)$$

where $\Gamma_1 = 1/(k_b^2 - \omega_c^2)$, $\Gamma_2 = 1/(4k_b^2 - \omega_c^2)$, $\bar{A}$ is the complex conjugate of A.

Substitute Eq. (26) and (25) into Eq. (24) yields

$$\begin{aligned} &D_0^2 q_2 + \omega_c^2 q_2 \\ &= +A^2\bar{A}\left[10a_3^2/3\omega_c^2 - 3a_4 - 4a_3\bar{a}_3/3\right] \\ &\quad \times exp(i\omega_c T_0) + i\bar{a}_5 f_1(k_a T_0) exp(i\omega_b T_0)/2 \\ &\quad - i\omega_c\left[2A' + 2\zeta A + \bar{a}_1 A f_1(k_a T_0)\right] exp(i\omega_c T_0) \\ &\quad - A^3(a_4 - 2a_3^2/3\omega_c^2 - 2a_3\bar{a}_3/3) exp(3i\omega_b T_0) \\ &\quad - (a_1/2 + a_3 a_5\Gamma_1 + \omega_c\bar{a}_2 f_2(k_a T_0)/2) A exp[i(k_b + \omega_c)T_0] \\ &\quad - (a_1/2 + a_3 a_5\Gamma_1 - \omega_c\bar{a}_2 f_2(k_a T_0)/2)\bar{A} exp[i(k_b - \omega_c)T_0] \\ &\quad - (a_2/2 + a_3(a_6 - \bar{a}_7 f_2(k_a T_0))\Gamma_2) A exp[i(2k_b + \omega_c)T_0] \\ &\quad - (a_2/2 + a_3(a_6 - \bar{a}_7 f_2(k_a T_0))\Gamma_2)\bar{A} exp[i(2k_b - \omega_c)T_0] \\ &\quad + cc \end{aligned} \quad (27)$$

It is well known that in a transmission tower-line system, large amplitude conductor vibration will be induced when one of excitation frequencies is very close to twice the critical natural frequency (sub-harmonic resonance). By solving Eq. (27), the amplitude of conductor vibration with sub-harmonic resonance can be calculated for the case considered here as follows. In this study, we defined that,

$$k_b = 2\omega_c + \varepsilon^2\sigma \quad (28)$$

Substitute Eq. (28) into Eq. (27) and remove secular terms in Eq. (27), yields

$$\begin{aligned} &A^2\bar{A}(10a_3^2/3\omega_c^2 - 3a_4 - 4a_3\bar{a}_3/3) \\ &\quad - i\omega_c(2A' + 2\zeta A + \bar{a}_1 A f_1(k_a T_0)) \\ &\quad - (a_1/2 + a_3 a_5\Gamma_1 - \omega_c\bar{a}_2 f_2(k_a T_0)/2)\bar{A} exp(i\varepsilon^2\sigma T_0) = 0 \end{aligned} \quad (29)$$

A in Eq. (29) is defined as polar form. Thus,

$$A = \chi exp(i\gamma)/2 \quad (30)$$

where χ is the amplitude and γ is phase angle, and both of them with respect to T_2.

Substitute Eq. (30) into Eq. (29), and separate it into the real and imaginary parts. Thus,

$$\begin{cases} \omega_c\chi' = -\omega_c\chi\kappa_1 - \chi\kappa_2 \sin\gamma \\ \omega_c\chi\gamma' = \omega_c\chi\sigma - \kappa_3\chi^3 - 2\chi\kappa_2\cos\gamma \end{cases} \quad (31)$$

where

$$\begin{aligned} \kappa_1 &= \zeta + \bar{a}_1 f_1(k_a T_0)/2 \\ \kappa_2 &= a_1/4 + a_3 a_5\Gamma_1/2 - \omega_c\bar{a}_2 f_2(k_a T_0)/4 \\ \kappa_3 &= 5a_3^2/6\omega_c^2 - 3a_4/4 - a_3\bar{a}_3/3 \\ \gamma &= \sigma T_2 - 2\psi \end{aligned}$$

Reduced equations of Eq. (31) governed the planar motion of the single conductor. which can be directly evoked by the combined forced and parametric excitation once the sub-harmonic resonance occurs.

For steady state, $\chi' = \gamma' = 0$, it can obtain the solution of the system by solving Eq. (31). Thus,

$$\omega_c^2\kappa_1^2 + (\omega_c\sigma + \kappa_3\chi^2)^2/4 = \kappa_2^2 \quad (32)$$

It can be easily derived from Eq. (32) that vibration amplitude varies depending on the detuning factor, excitation amplitude, initial tension and aerodynamic coefficients.

IV. CASE STUDY

Numerical studies are discussed here for a single conductor(which nearly the same one that described in [25]) of span $l = 400$ m, radius $R = 13.41$ mm, the mass per unit length $m = 1.35$kg, elastic modulus $E = 65\ GPa$, structural damping ratio $\xi_s = 0.1\%$. Initial tension $H = 55.05\ kN$, radius of the rivulet $r = 0.1R$, and yaw angle $\beta = 30^0$. The first order in-plane symmetric mode (Non-dimensional natural frequency) $\omega_c = 1.227$. The critical angle $\theta_c = 52^0$, where the measured drag coefficient has a sudden change from positive to negative. Thus, $40^0 < \theta \leq 70^0$, $C_{D0} = 0.8$, $C_{L1} = 0.85$ and $C_{L3} = -0.75$.

Firstly, effects of the upper rivulet position θ on the total damping ratio ξ is investigated, in absence ($s = 0$) or in presence ($s = 0.00375$) of the suspended insulator swing. As shown in Fig. 4, the zone between two curses of lower boundary and upper boundary ($s = 0$) is the uncoupled region which is affected only by aerodynamic force F_y, whereas the zone between two curses of lower boundary and upper boundary ($s = 0.00375$) is the coupled region which is affected by both of the aerodynamic force F_y and the suspended insulator swing B. From the comparison of these curves, it can be found that the upper rivulet position has obviously affect on the total damping ratio, which makes the total damping ratio starts to fluctuate in a certain range and negative values occur. Furthermore, the suspended insulator swing B modifies variation zone of the total damping ratio, which makes negative value is easier to appear.

The effects of the suspended insulator swing of small amplitude, with or without the upper rivulet, on response of the single conductor under sub-harmonic resonance are

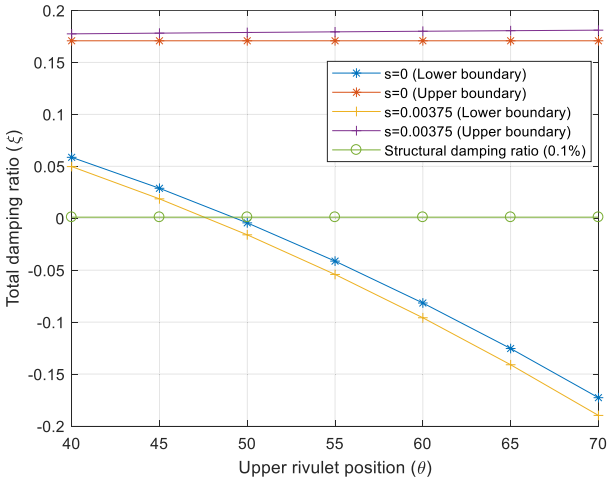

FIGURE 4. Total damping ratio ξ vs. upper rivulet position θ.

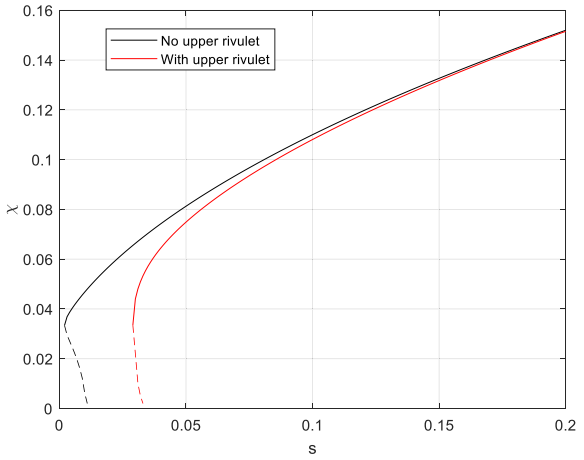

FIGURE 5. Amplitude χ vs. suspended insulator swing, in absence or presence of upper rivulet. Continuous line: stable; dashed line: unstable.

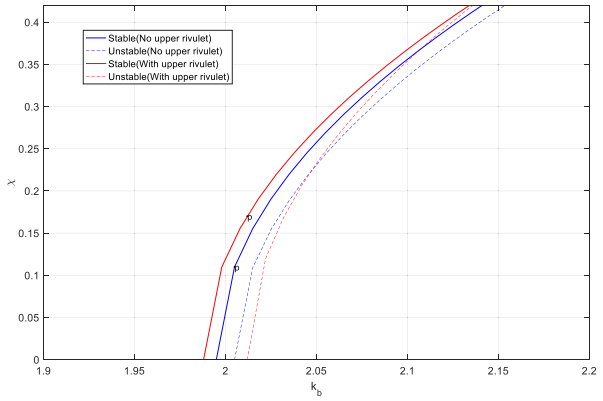

FIGURE 6. Frequency-response curves in absence or in presence of the upper rivulet when $s = 0.00375$ and $\xi_s = 0.1\%$.

illustrated (Fig. 5). The detuning is fixed at $\sigma = 0.01$, the upper rivulet position is $\theta = 50^0$ and the wind velocity is $U = 11$m/s. There is a clear difference between these two excitation-response curves. The sub-harmonic resonance of the single conductor at sole suspended insulator swing (i.e. In no upper rivulet condition) can be evoked even for a very small excitation. It can find that the response amplitude of the single conductor can reaches 0.0334 for the excitation is 0.002. The response amplitude will continue to increase with the excitation is increasing gradually. Moreover, the onset of sub-harmonic resonance in presence of the upper rivulet is relatively larger compared to that of sole suspended insulator swing. The response amplitude reaches 0.0335 for the excitation is 0.029. With the further increasing of excitation amplitude, the effect of the upper rivulet on the amplitude is gradually decreased and two excitation-response curves gradually tend to coincide with each other.

Fig. 6 shows the frequency-response curves in absence or in presence of the upper rivulet, for $s = 0.00375$ and $\xi_s = 0.1\%$. If excitation frequency ratio k_b is applied as a control parameter, there will have two curves of super-critical and sub-critical pitchfork bifurcations. In presence of the upper rivulet, the super-critical pitchfork bifurcation will occur at $k_b = 1.988$, whereas the sub-critical pitchfork bifurcation will occur at $k_b = 2.012$. For $k_b < 1.988$, there only has stable trivial solution available. For $1.988 < k_b < 2.012$, there is a stable non-trivial branch. For $k_b > 2.012$, two curves of a stable super-critical parabolic branch and an unstable sub-critical parabolic branch, both of them are occur. For the subs-critical pitchfork point ($k_b = 2.012$), there is a critical point p that separates the branch as two zones. The lower zone has large vibration response of the single conductor under sub-critical resonance with small perturbations, which is very dangerous to the single conductor for reason that it is easier to occur. The upper zone is the excessive vibration response of the single conductor under sub-critical resonance when the perturbations is higher or equal to response amplitude. The largest vibration would be happened during the single conductor is under coupling effects of the suspended insulator swing and other excitation, such as rain-wind aerodynamic forces.

By comparison of these curves, it can be found that upper rivulet enlarged space between the super-critical pitchfork bifurcation point and the sub-critical pitchfork bifurcation point. The response amplitude of the single conductor in presence of the upper rivulet is larger than that of the single conductor in absence of the upper rivulet. For example, when $k_b = 2$, the response amplitudes are 0.122(With upper rivulet) and 0.058(Without upper rivulet), respectively. This difference can be related to the effects of the upper rivulet on damping coupling and other terms in the governing equation.

Fig. 7 shows the time-domain dynamic response and phase plot of the single conductor with or without upper rivulet, for $s = 0.001$, $\xi_s = 0.1\%$, $\sigma = 0.01$ and $\theta_0 = 45^0$, calculated with Eq. (19) and (31) by a given displacement. It can be found that for a given displacement, the amplitude of the single conductor is decrease to a certain level when the angle θ reaches to critical angle of 52^0. Thus, ξ_a and ξ will change alternately from positive to negative value rather

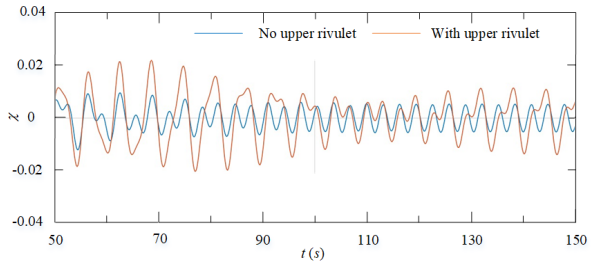

a Time evolution of the amplitude χ in absence or in presence of upper rivulet

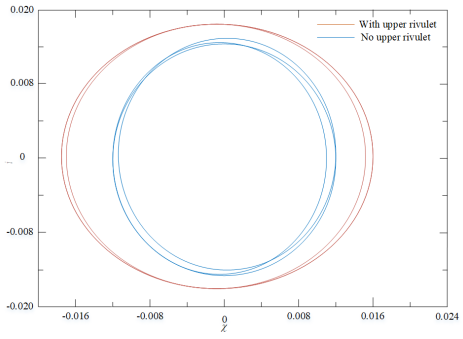

b Phase plot

FIGURE 7. Time evolution of the amplitude (a) and phase plot (b) in absence or in presence of upper rivulet, $s = 0.001$, $\xi_S = 0.1\%$ and $\sigma = 0.01$.

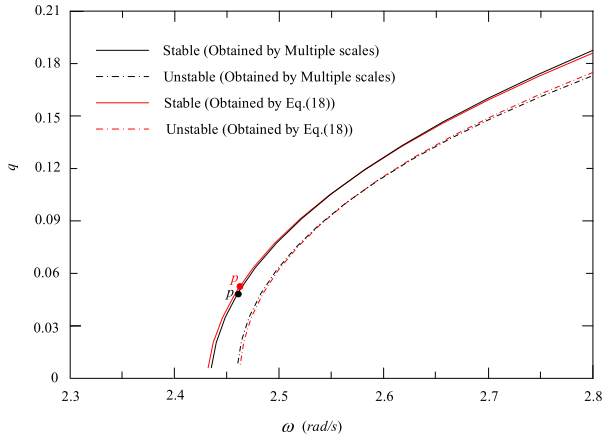

FIGURE 8. Frequency-Response curves of q in presence of the upper rivulet.

than keep constant. Accordingly, the motion of the single conductor with upper rivulet becomes almost periodic. The peak amplitude of the single conductor with upper rivulet in this case is higher than that of the single conductor without upper rivulet.

As shown in Fig. 8, frequency-Response curves of q in presence of the upper rivulet, for $s = 0.00375$ and $\xi_s = 0.1\%$. By comparison of this curves, it can be found that both of the stable and unstable response amplitudes of conductor computed by Multiple scales and Eq. (8) are very similar, which indicated the Multiple scales here can be used to reflect the nonlinear response of the conductor.

V. CONCLUSION

Analytical model for describing the nonlinear vibration of overhead power transmission conductor has proposed in this study. The effect of the upper rivulet position and the suspended insulator motion were applied in the model and be discussed. Some conclusions drawn as follows.

(1) Suspended insulators swing modified variation zone of the total damping ratio, which makes negative value easier to occur.

(2) Onset of sub-harmonic resonance in presence of the upper rivulet is relatively larger compared to that of sole suspended insulator swing. As the excitation amplitude increases, the effect of the upper rivulet on the amplitude gradually decreased and two excitation-response curves gradually tend to coincide with each other.

(3) Due to the upper rivulet, the space zone between super-critical and sub-critical pitchfork bifurcation points of the single conductor is extended. The response amplitude of the single conductor with upper rivulet is larger than that of the single conductor without upper rivulet.

(4) By a given an initial displacement, the amplitude of the single conductor is decrease to a certain level of which the aerodynamic damping ratio and the total damping ratio change alternately from positive to negative. the motion of the single conductor with upper rivulet becomes almost periodic and reduce slowly.

DECLARATIONS

Chao Zhou established the model and write the manuscript, and I reviewed the manuscript.

I confirm that I understand Scientific Reports is an open access journal that levies an article processing charge per articles accepted for publication. By submitting my article, I agree to pay this charge in full if my article is accepted for publication.

I declare that the authors have no competing interests as defined by Nature Research, or other interests that might be perceived to influence the results and/or discussion reported in this paper.

The results/data/figures in this manuscript have not been published elsewhere, nor are they under consideration (from you or one of your Contributing Authors) by another publisher.

I have read the Nature Research journal policies on author responsibilities and submit this manuscript in accordance with those policies.

REFERENCES

[1] G. Piccardo, L. C. Pagnini, and F. Tubino, "Some research perspectives in galloping phenomena: Critical conditions and post-critical behavior," *Continuum Mech. Thermodyn.*, vol. 27, no. 1, pp. 261–285, pp. 2015.

[2] M. Brahami, A. Gourbi, A. Tilmatine, and L. Dascalescu, "Numerical analysis of the induced corona vibrations on high-voltage transmission lines affected by rainfall," *IEEE Trans. Power Del.*, vol. 26, no. 2, pp. 617–624, Apr. 2011.

[3] C. Zhou, J. Yin, and Y. Liu, "Large swing behavior of overhead transmission lines under rain-load conditions," *Energies*, vol. 11, no. 5, p. 1092, Apr. 2018.

[4] K. S. Wang and G. J. Tang, "Response analysis of nonlinear vibration of overhead power line under suspension chain state," *J. Vib. Shock*, vol. 22, no. 2, pp. 69–72, 2003.
[5] S. W. Rienstra, "Nonlinear free vibrations of coupled spans of overhead transmission lines," *J. Eng. Math.*, vol. 53, nos. 3–4, pp. 337–348, Dec. 2005.
[6] R. Barbieri, N. Barbieri, and O. H. de Souza, Jr., "Dynamical analysis of transmission line cables. Part 3—Nonlinear theory," *Mech. Syst. Signal Process.*, vol. 22, no. 4, pp. 992–1007, May 2008.
[7] K. Q. Xia, Y. Liu, and Z. D. Qian, "Nonlinear dynamical response of high-voltage transmission lines based on cable dropping," *J. Southeast Univ. English Ed.*, vol. 25, no. 1, pp. 52–56 2009.
[8] W. Qin-Kuan, "Approximate solution of homotopic mapping for nonlinear vibration problem of transmission line," *Acta Phys. Sinica*, vol. 60, no. 6, 2011, Art. no. 068802.
[9] Z. Yan, Z. Yan, Z. Li, and T. Tan, "Nonlinear galloping of internally resonant iced transmission lines considering eccentricity," *J. Sound Vib.*, vol. 331, no. 15, pp. 3599–3616, Jul. 2012.
[10] X. Liu and B. Huo, "Nonlinear vibration and multimodal interaction analysis of transmission line with thin ice accretions," *Int. J. Appl. Mech.*, vol. 07, no. 01, Feb. 2015, Art. no. 1550007.
[11] D. Wang, X. Chen, and J. Li, "Prediction of wind-induced buffeting response of overhead conductor: Comparison of linear and nonlinear analysis approaches," *J. Wind Eng. Ind. Aerodyn.*, vol. 167, pp. 23–40, Aug. 2017.
[12] M. Zhang, G. Zhao, and J. Li, "Nonlinear dynamic analysis of high-voltage overhead transmission lines," *Shock Vib.*, vol. 2018, Apr. 2018, Art. no. 1247523.
[13] F. Alminhana, M. Mason, and F. Albermani, "A compact nonlinear dynamic analysis technique for transmission line cascades," *Eng. Struct.*, vol. 158, pp. 164–174, Mar. 2018.
[14] A. H. P. Van der Burgh, "Rain-wind-induced vibrations of a simple oscillator," *Int. J. Non-Linear Mech.*, vol. 39, no. 1, pp. 93–100, 2004.
[15] A. H. P. Van der Burgh and A. K. Abramian, "A new model for the study of rain-wind-induced vibrations of a simple oscillator," *Int. J. Non-Linear Mech.*, vol. 43, no. 1, pp. 345–358, 2006.
[16] X. Fu and H.-N. Li, "Dynamic analysis of transmission tower-line system subjected to wind and rain loads," *J. Wind Eng. Ind. Aerodyn.*, vol. 157, pp. 95–103, Oct. 2016.
[17] X. Fu and H.-N. Li, "Effect of raindrop size distribution on rain load and its mechanism in analysis of transmission towers," *Int. J. Struct. Stability Dyn.*, vol. 18, no. 09, Sep. 2018, Art. no. 1850115.
[18] C. Zhou, Y. Liu, and Z. Ma, "Investigation on aerodynamic instability of high-voltage transmission lines under rain-wind condition," *J. Mech. Sci. Technol.*, vol. 29, no. 1, pp. 131–139, Jan. 2015.
[19] C. Zhou, J. Yin, and Y. Liu, "Effects of wind and rain on the motion of the high-voltage conductor in a simplified valley terrain," *Electr. Power Syst. Res.*, vol. 173, pp. 153–163, Aug. 2019.
[20] C. Seidel and D. Dinkler, "Rain–wind induced vibrations–phenomenology, mechanical modelling and numerical analysis," *Comput. Struct.*, vol. 84, nos. 24–25, pp. 1584–1595, Sep. 2006.
[21] Q. C. Zhang, W. Y. Li, and W. Wang, "Nonlinear dynamic behavior of rain-wind-induced vibration of a stay cable," *J. Vib. Shock*, vol. 29, no. 4, pp. 173–176, 2010.
[22] M. Rafei and W. T. Van Horssen, "Solving systems of nonlinear difference equations by the multiple scales perturbation method," *Nonlinear Dyn.*, vol. 69, no. 4, pp. 1509–1516, Sep. 2012.
[23] T. Wu, A. Kareem, and S. Li, "On the excitation mechanisms of rain–wind induced vibration of cables: Unsteady and hysteretic nonlinear features," *J. Wind Eng. Ind. Aerodyn.*, vol. 122, pp. 83–95, Nov. 2013.
[24] C. Zhou, Y.-P. Liu, and Y.-W. Song, "Mechanism and modeling of rain-wind induced in-plane vibration on high-voltage transmission line," *J. Mech. Sci. Technol.*, vol. 28, no. 4, pp. 1175–1180, Apr. 2014.
[25] C. Zhou and Y. P. Liu, "A theoretical model of rain-wind-induced in-plane galloping on overhead transmission tower-lines system," *Adv. Mech. Eng.*, vol. 7, no. 9, pp. 1–10, 2015.
[26] C. Zhou and J. Yin, "Effects of time-varying mass on stability of high-voltage conductor in Rain–Wind condition," *J. Comput. Nonlinear Dyn.*, vol. 15, no. 5, May 2020, Art. no. 051001.

CHAO ZHOU was born in Hanzhong, Shanxi, China, in 1980. He received the B.S. degree in mechanical engineering from Wuhan Textile University, Wuhan, in 2005, and the Ph.D. degree in mechanical engineering from Wuhan University, Wuhan, in 2010.

In 2010, he joined the School of Energy, Power and Mechanical Engineering, North China Electric Power University, Beijing, China, as a Lecturer, and in 2015 became an Associate Professor. His current research interests include high-voltage conductor galloping, time-varying mass vibration, and nonlinear vibration.

Dr. Zhou was a member of the National Ground Wire Standardization Technical Committee, China, in 2019.